

**On the effects of the final state interaction in the
electro-disintegration of the deuteron at intermediate and high
energies**

C. Ciofi degli Atti, L.P. Kaptari *

*Department of Physics, University of Perugia, and INFN, Sezione di Perugia, via A. Pascoli,
Perugia, I-06100, Italy*

D. Treleani

*Department of Theoretical Physics, University of Trieste, Strada Costiera 11, INFN, Sezione di
Trieste and ICTP, I-34014 Trieste, Italy*

(November 2, 2018)

arXiv:nucl-th/0005027v1 10 May 2000

Typeset using REVTeX

*On leave from Bogoliubov Lab. Theor. Phys., JINR, Dubna, Russia.

Abstract

The role of the final state interactions (FSI) in the inclusive quasi-elastic disintegration of the deuteron is investigated treating the two-nucleon final state within the exact continuum solutions of the non-relativistic Schroedinger equation, as well as within the Glauber multiple scattering approach. It is shown that for values of the Bjorken scaling variable $x_{Bj} \simeq 1$ both approaches provide similar results, unless the case $x_{Bj} \gtrsim 1$, where they appreciably disagree. It is demonstrated that present experimental data, which are mostly limited to a region of four-momentum transfer ($Q^2 \lesssim 4(\text{GeV}/c)^2$) where the Center-of-Mass energy of the final state is below the pion threshold production, can be satisfactorily reproduced by the approach based on the exact solution of the Schroedinger equation and not by the Glauber approach. It is also pointed out that the latter, unlike the former, does not satisfy the inelastic Coulomb sum rule, the violation being of the order of about 20%.

I. INTRODUCTION

The role played by the effects of final state interaction (FSI) in electro-disintegration processes is a very relevant issue, for they may in principle hinder the extraction of reliable information not only on nuclear structure, but also on fundamental hadronic properties in the medium, which could be obtained from different kinds of lepton scattering processes off nuclear targets. Apart from the few-body systems at low energies, for which exact solutions of the Schroedinger equation in the continuum are becoming to be available (see e.g. [1,2]), the treatment of FSI effects in complex systems at intermediate and high energies still requires the use of several approximations. This concerns both the semi-inclusive processes $A(e, e'p)X$ (see e.g. [3]), and the fully inclusive process $A(e, e')X$, for which several methods have been proposed with conflicting results (see e.g. [4]). Most of these approaches rely on the use of the Glauber multiple scattering theory, assuming that the struck nucleon, after γ^* absorption, is on shell and propagates in the medium with total energy $\sqrt{(\mathbf{q} + \mathbf{p})^2 + M^2} \simeq \sqrt{\mathbf{q}^2 + M^2}$ (\mathbf{q} and \mathbf{p} are the three-momentum transfer and the momentum of the struck nucleon before interaction, respectively). The latter assumption, which is a very reasonable one at $x_{Bj} \simeq 1$ ($x_{Bj} = Q^2/(2M\nu)$ is the Bjorken scaling variable [5], $Q^2 = \mathbf{q}^2 - \nu^2$ the four-momentum transfer, and M the nucleon mass), could be questionable at higher or lower values of x_{Bj} , where the struck nucleon, after γ^* absorption, is far off-shell; moreover, even at high values of $|\mathbf{q}|$, the two nucleon relative energy might be not sufficiently high to justify the use of the Glauber high energy approximation, so that a careful consideration of the two-nucleon kinematics is called for. As a matter of fact, it has been shown [6] that existing data on the inclusive electro-disintegration of the deuteron, $D(e, e')X$ [7], correspond, at $x_{Bj} > 1$, to a very low relative energy of the two nucleon final state even if $|\mathbf{q}|$ is very large, and that they can be satisfactorily explained by using for the continuum state the solution

of the non relativistic Schroedinger equation ¹. It is however clear that, given a fixed value of x_{Bj} , if $|\mathbf{q}|$ (i.e. Q^2) is further increased, inelastic processes could become operative and the Schroedinger approach becomes inadequate. Within these kinematical conditions, i.e. at high relative energies of the np -pair in the continuum, the Glauber approach has been frequently used to calculate FSI effects, which, however, requires several approximations in case of complex nuclei. In the deuteron case, FSI effects can be calculated exactly within both the Schroedinger and the Glauber approaches. It is just the aim of this paper to present the results of such a calculation for the inclusive electro-disintegration of the deuteron $D(e, e')X$ in the quasi-elastic region, i.e. at $\nu \leq Q^2/2M$, or $x_{Bj} > 1$. In order to better display the effects of the FSI, our results will be presented not only in terms of cross sections, but also in terms of y-scaling functions [6]. Our paper is organized as follows: in Chapter II the basic formalism of inclusive processes within the Plane Wave Impulse Approximation (PWIA) is recalled; the formalism pertaining to the treatment of the FSI within the Schroedinger and the Glauber approaches is illustrated in Chapter III; the results of calculations are given in Chapter IV; the Conclusions are drawn in Chapter V.

II. THE ONE PHOTON EXCHANGE AND THE PLANE WAVE IMPULSE APPROXIMATIONS

In this Section the relevant formulae describing the inclusive cross section $D(e, e')X$ will be recalled. In the One Photon Exchange Approximation, depicted in fig.1, the inclusive cross section reads as follows

$$\frac{d^3\sigma}{d\Omega'd\mathcal{E}'} = \sum_f |\langle \mathbf{P}_f, f | \hat{O} | i, \mathbf{P}_i \rangle|^2 \delta(\nu + \varepsilon_i - \varepsilon_f), \quad (2.1)$$

where $|i\rangle$ and $|f\rangle$ are the initial and final eigenfunctions of the intrinsic nuclear Hamiltonian, $\hat{O} = K \cdot j_\mu \frac{1}{Q^2} J^\mu$, j_μ and J_μ are the electromagnetic currents of the electron and the deuteron, respectively, and K is a kinematical factor (see below).

The 4-momenta of the initial and final electrons in the laboratory system are $k = (\mathcal{E}, \mathbf{k})$ and $k' = (\mathcal{E}', \mathbf{k}')$, respectively, the four momentum transfer is $q = k - k' = (\nu, \mathbf{q})$, and the orientation of the coordinate system is defined by $\mathbf{q} = (0, 0, q_z)$.

At high energies the electron mass can be disregarded, so that

$$k^2 = (k')^2 \simeq 0, \quad kk' = -kq = \frac{-q^2}{2} = \frac{Q^2}{2}, \quad (2.2)$$

$$Q^2 \equiv -q^2 = 4\mathcal{E}\mathcal{E}' \sin^2 \frac{\theta}{2}. \quad (2.3)$$

where θ is the scattering angle. The following relations will be used in what follows:

¹From now on, the method based upon the exact solution of the non-relativistic Schroedinger equation to generate bound and continuum two-nucleon states, will be referred to as the *Schroedinger approach*

$$\mathcal{E} = \frac{\nu}{2} \left(1 + \frac{\sqrt{\sin^2 \frac{\theta}{2} + \frac{Q^2}{\nu^2}}}{\sin \frac{\theta}{2}} \right), \quad \mathcal{E}' = \mathcal{E} - \nu \quad (2.4)$$

$$|\mathbf{q}| = |q_z| = \sqrt{Q^2 + \nu^2}. \quad (2.5)$$

In PWIA, depicted in fig. 2, the three-nucleon momenta in the deuteron, before interaction, are $\mathbf{p}_1 = -\mathbf{p}_2$ and, after interaction, $\mathbf{p}_1' = \mathbf{q} + \mathbf{p}_1$ and $\mathbf{p}_2' = \mathbf{p}_2$; the relative and center of mass (CM) momenta are $\mathbf{p} = (1/2)(\mathbf{p}_1 - \mathbf{p}_2) = \mathbf{p}_1$ and $\mathbf{P} = (\mathbf{p}_1 + \mathbf{p}_2) = 0$. The PWIA cross section in the lab system has the following form ($\mathbf{p}_1 = -\mathbf{p}_2$):

$$\frac{d^3\sigma}{d\Omega' d\mathcal{E}'} = \int \sigma_{Mott} \sum_{N_i=1,2} \left[V_L |\langle p_1 | \hat{J}_L^{N_i}(Q^2) | p_1' \rangle|^2 + V_T |\langle p_1 | \hat{J}_T^{N_i}(Q^2) | p_1' \rangle|^2 \right] \times \left[\frac{M^2 d\mathbf{p}_2}{E_1 E_2} \delta(M_D + \nu - E_1' - E_2) \right] n(|\mathbf{p}|), \quad (2.6)$$

where $L(T)$ refer to the longitudinal (transverse) part of the nucleon current operator, $V_{L(T)}$ are the corresponding well-known kinematical factors ($V_L = \frac{Q^4}{|\mathbf{q}|^4}$, $V_T = \tan^2(\theta/2) + \frac{Q^2}{2|\mathbf{q}|^2}$), and $n^D(|\mathbf{p}|)$ is the nucleon momentum distribution in the deuteron

$$n^D(|\mathbf{p}|) = \frac{1}{3(2\pi)^3} \sum_{\mathcal{M}_D} \left| \int \Psi_{1,\mathcal{M}_D}(\mathbf{r}) \exp(i\mathbf{p}\mathbf{r}) d\mathbf{r} \right|^2, \quad (2.7)$$

where $\Psi_{1,\mathcal{M}_D}^D(\mathbf{r})$ is the non relativistic deuteron wave function, with the two nucleon relative co-ordinate given by $\mathbf{r} = \mathbf{r}_1 - \mathbf{r}_2$. It is a common practice to express the cross section (2.6) in terms of the free electron-nucleon cross section for an on mass-shell nucleon, i.e. to extrapolate the Rosenbluth cross section to the off-mass shell case [8]. Since energy conservation in the two cases is different (whereas the three momentum conservation is the same) the extrapolation unavoidably requires additional, *ad hoc* assumptions. In this paper we adopt the prescription of [8], according to which the hit nucleon is considered to be on-shell, i.e. with a four momentum equal to the one of a free nucleon, *viz.* $p_1^{on} = (\sqrt{\mathbf{p}_1^2 + M^2}, \mathbf{p}_1)$, and in (2.6) the replacement $\nu \rightarrow \bar{\nu} = \nu + M_D - \sqrt{M^2 + \mathbf{p}_1^2} - \sqrt{M^2 + \mathbf{p}_2^2}$ is done, so that $\delta(M_D + \nu - E_1' - E_2) \rightarrow \delta(\sqrt{\mathbf{p}_1^2 + M^2} + \bar{\nu} - E_1')$; by this way, the electromagnetic vertex of the nuclear tensor corresponds to that of a free nucleon, evaluated at the same \mathbf{q} , but at the transferred energy $\bar{\nu}$ instead of ν , which means that the nucleon hadronic tensor has to be evaluated for $p_N = p_N^{on}$ and $Q_N^2 = \bar{Q}^2 = \mathbf{q}^2 - \bar{\nu}^2 \neq Q^2$. By such a procedure one obtains

$$\begin{aligned} \frac{d^3\sigma}{d\Omega' d\mathcal{E}'} &= \int \bar{\sigma}_{eN} n^D(|\mathbf{p}|) d\mathbf{p} \delta(\bar{\nu} + \sqrt{M^2 + \mathbf{p}^2} - \sqrt{M^2 + (\mathbf{p} + \mathbf{q})^2}) = \\ &= (2\pi) \int_{|y|}^{p_{max}} \bar{\sigma}_{eN} \frac{E_{\mathbf{p}+\mathbf{q}}}{|\mathbf{q}|} n^D(|\mathbf{p}|) |\mathbf{p}| d|\mathbf{p}|, \end{aligned} \quad (2.8)$$

where $\bar{\sigma}_{eN}$ is the extrapolated electron -nucleon cross section for an off-mass shell nucleon [8], $E_{\mathbf{p}+\mathbf{q}} = E_1' = \sqrt{M^2 + (\mathbf{p} + \mathbf{q})^2}$, and the limits of integration, which are obtained from the energy conservation provided by the δ - function, are as follows

$$|\mathbf{p}|_{min} = \frac{1}{2} \left| \left\{ (M_D + \nu) \sqrt{1 - \frac{4m^2}{s}} - |\mathbf{q}| \right\} \right| \equiv |y| \quad (2.9)$$

$$|\mathbf{p}|_{max} = \frac{1}{2} \left\{ (M_D + \nu) \sqrt{1 - \frac{4m^2}{s}} + |\mathbf{q}| \right\} \equiv p_{max}, \quad (2.10)$$

where s denotes the Mandelstam variable for the $\gamma^* D$ vertex

$$s = (P_D + q)^2 = M_D(M_D + 2\nu) - Q^2. \quad (2.11)$$

and y is the scaling variable according to [6]

$$y = \frac{1}{2} \left\{ |\mathbf{q}| - (M_D + \nu) \sqrt{1 - \frac{4m^2}{s}} \right\} \quad (2.12)$$

When the value of $|\mathbf{q}|$ becomes large enough, one has $p_{max} \sim \infty$ and the dependence of $\bar{\sigma}_{eN}$ upon $|\mathbf{p}|$ becomes very weak. In such a case eq. (2.8) can be cast in the following form [6]

$$\frac{d\sigma}{d\Omega' d\mathcal{E}'} = (s_{ep} + s_{en}) \frac{E_{y+|\bar{q}|}}{|\mathbf{q}|} (2\pi) \int_{|y|}^{\infty} |\mathbf{p}| d|\mathbf{p}| n^D(|\mathbf{p}|), \quad (2.13)$$

where s_{eN} and $E_{y+|\bar{q}|}$ represent $\bar{\sigma}_{eN}$ and $E_{\bar{p}+\bar{q}}$, calculated at $|\mathbf{p}| = |\mathbf{p}|_{min} = |y|$, and can therefore be taken out of the integral. Such an approximation, which has been carefully investigated in ref. [6], turns out to be valid within few percents, provided $Q^2 > 0.5 GeV^2/c^2$. It is clear therefore, that at large values of $|\mathbf{q}|$ the following quantity (the *non relativistic scaling function*)

$$F(|\mathbf{q}|, y) \equiv \frac{|\mathbf{q}|}{E_{y+|\bar{q}|}} \cdot \left(\frac{d\sigma}{d\Omega' d\mathcal{E}'} \right) / (s_{ep} + s_{en}) \quad (2.14)$$

will be directly related to the longitudinal momentum distribution

$$F(|\mathbf{q}|, y) \longrightarrow f(y) = 2\pi \int_{|y|}^{\infty} |\mathbf{p}| d|\mathbf{p}| n^D(|\mathbf{p}|), \quad (2.15)$$

Thus the condition for the occurrence of non relativistic y -scaling is that eq. (2.8) could be cast in the form (2.13), which means that: i) $Q^2 > 0.5 GeV^2/c^2$, in order to make the replacement $\bar{\sigma}_{eN} \rightarrow s_{eN}$ and $E_{\bar{p}+\bar{q}} \rightarrow E_{y+|\bar{q}|}$ possible, and ii) $p_{max} = (|\mathbf{q}| - |y|) \gg |y|$ (cf. (2.9) and (2.10)) in order to saturate the integral of the momentum distribution, $\int_{|y|}^{p_{max}} |\mathbf{p}| d|\mathbf{p}| n^D(|\mathbf{p}|) \rightarrow \int_{|y|}^{\infty} |\mathbf{p}| d|\mathbf{p}| n^D(|\mathbf{p}|)$. Condition ii) obviously implies that the larger the value of $|y|$, the larger the value of $|\mathbf{q}|$ at which scaling will occur. The satisfaction of the inequalities $|\mathbf{q}| \gg 2|y|$, $x_{Bj} > 1$ leads, for any well-behaved $n(|\mathbf{p}|)$, to the following conditions for the occurrence of non relativistic y -scaling:

$$2m/3 \lesssim \nu < |\mathbf{q}|, \quad |\mathbf{q}| \gtrsim 2m. \quad (2.16)$$

Note, that the above conditions are very different from the conditions for Bjorken scaling $\nu \simeq |\mathbf{q}|$.

III. THE FINAL STATE INTERACTION

A. The Schroedinger Approach

In the calculation of the FSI, depicted in Fig. 3, it is more convenient to perform calculations in the frame where the interacting np -pair in the final state is at rest. The phase-space factor can be written as follows

$$\frac{d\mathbf{p}'_1 d\mathbf{p}'_2}{E'_1 E'_2} \delta^{(4)}(P_D + q - P_f) = \frac{d\mathbf{P}_f d\mathbf{p}_{rel}}{2E^{*2}} \delta^{(3)}(\mathbf{q} - \mathbf{P}_f) \delta\left(E^* - \frac{\sqrt{s}}{2}\right), \quad (3.1)$$

where \mathbf{p}_{rel} is the relative momentum of the np -pair which is defined by the Mandelstam variable $s = 4(\mathbf{p}_{rel}^2 + M^2)$. For the longitudinal current one has

$$G_E(Q^2) \exp(i\mathbf{q}\mathbf{r}/2) = (4\pi)^2 G_E(Q^2) \sum_{\lambda,\mu} i^\lambda j_\lambda(qr/2) Y_{\lambda\mu}^*(\hat{\mathbf{q}}) Y_{\lambda\mu}(\hat{\mathbf{r}}) \equiv (4\pi)^2 G_E(Q^2) \sum_{\lambda,\mu} Y_{\lambda\mu}^*(\hat{\mathbf{q}}) \hat{O}_{\lambda\mu}. \quad (3.2)$$

with $\hat{O}_{\lambda\mu} = i^\lambda j_\lambda(qr/2) Y_{\lambda\mu}(\hat{\mathbf{r}})$, and the corresponding cross section is

$$\frac{d^3\sigma^L}{d\Omega' d\mathcal{E}'} = \frac{4}{3} \frac{M^2 \sigma_{Mott}}{2\pi} V_L G_E(Q^2)^2 \sum_{J_f} \sum_{\lambda} \left| \langle J_D || \hat{O}_{\lambda}(|\mathbf{q}|) || p_{rel}; J_f L_f S_f \rangle \right|^2 \frac{|\mathbf{p}_{rel}|}{\sqrt{s}}. \quad (3.3)$$

where the radial part of the two-nucleon wave function in the continuum $|p_{rel}; J_f L_f S_f\rangle$ has the following behaviour

$$u_{LS}^J(r) \xrightarrow{r \rightarrow \infty} \frac{1}{p_{rel}} \sin\left(p_{rel} r - \frac{L\pi}{2} + \delta_L\right). \quad (3.4)$$

It can be seen that equation (3.3) differs from the PWIA result (2.8). However, by using the identity $\frac{1}{2|\mathbf{q}|} \int_{|y|}^{p_{max}} \frac{|\mathbf{p}| d|\mathbf{p}|}{E} = \frac{p_{rel}}{\sqrt{s}}$ one may cast the cross section in the following form

$$\frac{d\sigma^L}{d\Omega' d\mathcal{E}'} = (s_{ep} + s_{en})^L \frac{E_{y+|\vec{q}|}}{|\mathbf{q}|} \int_{|y|}^{p_{max}} |\mathbf{p}| d|\mathbf{p}| n_S^D(|\mathbf{p}|, |\mathbf{q}|, \nu), \quad (3.5)$$

where, the following quantity has been introduced

$$n_S^D(|\mathbf{p}|, |\mathbf{q}|, \nu) = \frac{1}{4\pi} \frac{1}{3} \sum_{J_f} \sum_{\lambda} \left| \langle J_D || \hat{O}_{\lambda}(|\mathbf{q}|) || p_{rel}; J_f L_f S_f \rangle \right|^2, \quad (3.6)$$

B. The Glauber Approach

In the Glauber approach the exact two-nucleon continuum wave function $|f\rangle$ is approximated by its eikonal form. Then the cross section can be written in the same form as equation (2.8) with the deuteron momentum distribution (2.7) replaced by the Glauber distorted momentum distribution n_G^D [9],

$$n^D(\mathbf{p}) \rightarrow n_G^D(\mathbf{p}_m) = \frac{1}{3} \frac{1}{(2\pi)^3} \sum_{\mathcal{M}_D} \left| \int d\mathbf{r} \Psi_{1,\mathcal{M}_D}^*(\mathbf{r}) S(\mathbf{r}) \chi_f \exp(-i\mathbf{p}_m \mathbf{r}) \right|^2, \quad (3.7)$$

where

$$\mathbf{p}_m = \mathbf{q} - \mathbf{p}'_1 \quad (3.8)$$

is the missing momentum, χ_f the spin wave function of the final np -pair and $S(\mathbf{r})$ the S -matrix describing the final state interaction between the hit nucleon and the spectator, *viz.* (see Ref. [9])

$$S(\mathbf{r}) = 1 - \theta(z) \Gamma_{el}(\mathbf{b}), \quad (3.9)$$

with the elastic profile function $\Gamma_{el}(\mathbf{b})$ being

$$\Gamma_{el}(\mathbf{b}) = \frac{\sigma_{tot}(1 - i\alpha)}{4\pi b_0^2} \exp(-b^2/2b_0^2). \quad (3.10)$$

In eqs. (3.9) and (3.10) $\mathbf{r} = \mathbf{b} + z\mathbf{q}/|\mathbf{q}|$ defines the longitudinal, z , and the perpendicular, \mathbf{b} , components of the relative coordinate \mathbf{r} , $\sigma_{tot} = \sigma_{el} + \sigma_{in}$, α is the ratio of the real to the imaginary part of the forward elastic pn scattering amplitude, and, eventually, the step function $\theta(z)$ originates from the Glauber's high energy approximation, according to which the struck nucleon propagates along a straight-line trajectory and can interact with the spectator only provided $z > 0$. The following relations will be useful in what follows

$$\sigma_{el} = \int |\Gamma_{el}(\mathbf{b})|^2 d^2b = \frac{\sigma_{tot}^2(1 + \alpha^2)}{16\pi b_0^2} \quad (3.11)$$

$$f_{el}(\Delta_\perp) = \frac{ik}{2\pi} \frac{\sigma_{tot}(1 - i\alpha)}{4\pi b_0^2} \int d^2b e^{i\Delta_\perp \mathbf{b}} e^{-b^2/2b_0^2} = \frac{ik}{4\pi} \sigma_{tot}(1 - i\alpha) e^{-b_0^2 \Delta_\perp^2/2} \quad (3.12)$$

$$\frac{d\sigma_{el}}{d^2\Delta} = \frac{1}{k^2} |f_{el}(\Delta)|^2 = \frac{\sigma_{tot}^2(1 + \alpha^2)}{16\pi^2} \exp(-b_0^2 \Delta_\perp^2) \quad (3.13)$$

where Δ is the transferred momentum in the $N - N$ collision, and

$$b_0^2 = \frac{\sigma_{tot}^2(1 + \alpha^2)}{16\pi\sigma_{el}} \quad (3.14)$$

is the slope of the q -dependence of the elastic proton-neutron cross section. Assuming that at high relative energies of the np -pair the differences between the absorption of longitudinal (L) and transverse (T) photons connected with the spin dependence of FSI effects can be disregarded, eq.(2.13) becomes

$$\frac{d\sigma}{d\Omega' d\mathcal{E}'} = (s_{ep} + s_{en}) \frac{E_{y+|\vec{q}|}}{|\mathbf{q}|} (2\pi) \int_{|y|}^{p_{max}} |\mathbf{p}_m| d|\mathbf{p}_m| n_G^D(|\mathbf{p}_m|, \cos\theta_{\mathbf{q}\mathbf{p}_m}). \quad (3.15)$$

It should be stressed, first, that in absence of any FSI, the distorted momentum distribution $n_G^D(\mathbf{p}_m)$ reduces to the undistorted momentum distribution $n^D(\mathbf{p})$ ($\mathbf{p}_m = -\mathbf{p}_1$) and, secondly, that unlike $n^D(\mathbf{p})$, $n_G^D(\mathbf{p}_m)$ depends also upon the orientation of \mathbf{p}_m with respect to the momentum transfer \mathbf{q} , with the angle $\theta_{\mathbf{q}\mathbf{p}_m}$ being fixed by the energy conserving δ -function, namely $\cos \theta_{\mathbf{q}\mathbf{p}_m} = [(2(M_D + \nu)\sqrt{|\mathbf{p}_m|^2 + M^2 - s})]/(2|\mathbf{q}||\mathbf{p}_m|)$; thus $n_G^D(\mathbf{p}_m)$ depends implicitly on the kinematics of the process, and the values of y and $|\mathbf{q}|$ fix the value of the total energy (2.11) of the final np pair, i.e. the relative energy of the nucleons in the final states. Consequently, the quantities σ_{tot} , α and b_0 in (3.10) also depend upon the kinematics of the process. In this sense, the distorted momentum distribution $n_G^D(\mathbf{p}_m)$ implicitly depends upon $|\mathbf{q}|$ and y as well.

C. The longitudinal sum rule

Let us now briefly discuss the charge conservation sum rule in the quasi-elastic processes. The longitudinal part of the hadronic current is the charge density of the target and the longitudinal cross section may be written in the form

$$\frac{d^3\sigma^L}{d\Omega'd\mathcal{E}'} = \int \frac{V_L}{3} \sum_{\mathcal{M}_D, \mathcal{J}_f, \mathcal{M}_f} |\langle P_D, \mathcal{M}_D | \hat{J}_L^D(Q^2) | P_f, \mathcal{M}_f \rangle|^2 \left[\frac{d\mathbf{p}_2}{(2\pi)^3} \delta(\nu + E_i - E_f) \right]. \quad (3.16)$$

Integrating over the energy loss ν , summing over the final states and, disregarding, for ease of presentation, the neutron form factor G_E^n , the longitudinal sum rule can be obtained (see for details ref. [10])

$$\mathcal{S} = \int (G_E^2(Q^2) V_L)^{-1} \frac{d^3\sigma^L}{d\Omega'd\mathcal{E}'} d\nu = \frac{1}{3} \sum_{\mathcal{M}_D} \int \left| \int \Psi_{1,\mathcal{M}}(\mathbf{r}) \exp(i\mathbf{p}\mathbf{r}) d\mathbf{r} \right|^2 \frac{d\mathbf{p}}{(2\pi)^3} = 1. \quad (3.17)$$

Note that the sum over the final states contains also the contribution from elastic scattering, so that in order to obtain the longitudinal sum rule corresponding to the inelastic scattering the elastic part, $F_p^2(Q^2) = |\langle D | \exp(i\mathbf{q}\mathbf{r}_p) | D \rangle|^2$, has to be subtracted from eq. (3.17), obtaining

$$\mathcal{S}_{in} = \lim_{Q^2 \rightarrow \infty} (\mathcal{S} - F_p^2(Q^2)) \longrightarrow 1. \quad (3.18)$$

The longitudinal sum rule (3.18) is fulfilled exactly within the PWIA, as well as when the Schroedinger approach is used to include the FSI; if the latter are considered within the Glauber approach, as described in the previous paragraph, the sum rule is not satisfied. As a matter of fact by using eqs. (3.11)-(3.14) and introducing the inelastic profile function $\Gamma_{inel}(\mathbf{b})$ through the unitarity relation

$$2Re \Gamma_{el}(\mathbf{b}) = \Gamma_{el}(\mathbf{b}) + \Gamma_{inel}(\mathbf{b}), \quad (3.19)$$

one obtains

$$\mathcal{S}_{in} = \int d\mathbf{r} |\Psi_{1,\mathcal{M}}(\mathbf{r})|^2 \left(1 - \theta(z) |\Gamma_{inel}(\mathbf{b})|^2 \right), \quad (3.20)$$

which shows that if the inelastic channels are absent, the longitudinal sum rule (3.17) is fulfilled, whereas in the presence of open inelastic channels one has $\mathcal{S}_{in} < 1$, i.e. the incident nucleon flux is partially absorbed by inelastic processes.

IV. RESULTS OF CALCULATIONS

A. The Schroedinger approach.

The calculation of the cross section and the scaling function by eqs. (3.5) and (2.14), requires the knowledge of the wave functions $|p_{rel}; J_f L_f S_f\rangle$ of the final np -pair, which are solutions of the Schroedinger equation in the continuum with a given nucleon-nucleon potential. It is well known that the non relativistic deuteron momentum distributions calculated with different realistic potentials, *viz.* the Bonn [12], Paris [13] and Reid [14] ones, exhibit rather different behaviours at moderate and large momenta. It has also been shown that relativistic calculations of the deuteron momentum distribution within the Bethe-Salpeter formalism, yield results which are very close to those obtained with the Reid Soft Core (RSC) potential (see ref. [11]). Therefore we have used the RSC potential to solve the Schroedinger equation for the $|p_{rel}; J_f L_f S_f\rangle$ states, taking into account all partial waves with $J_f < 3$. For higher values of J_f the PWIA has been adopted. For the sake of comparison with the experimental data we have also assumed that the effects of the FSI on the longitudinal and transverse parts of the cross section is the same, and is governed by the quantity (3.6). In the Schroedinger approach, FSI arise from the elastic rescattering of the two nucleons in the final states. The threshold for inelastic channels corresponds to a value of the total energy of the np -pair $\sqrt{s} \gtrsim 2 \text{ GeV}$, or equivalently, $p_{lab} \gtrsim 0.8 \text{ GeV}/c$, where p_{lab} is the laboratory momentum of the struck nucleon (i.e. with the spectator at rest), corresponding to a total energy $\sqrt{s} = \sqrt{2M^2 + 2M\sqrt{p_{lab}^2 + M^2}}$. Experimentally [15], the inelastic channel contribution starts to be relevant at $p_{lab} \simeq 1.2 \text{ GeV}/c$. The inclusive $D(e, e')X$ cross section corresponding to electron beam energy $\mathcal{E} = 9.761 \text{ GeV}$ and scattering angle $\theta = 10^\circ$ is shown in fig. 4. The dotted line corresponds to the PWIA and the solid curve is the result which includes the FSI. It can be seen that in the range $0.8 \text{ GeV} < \nu < 1.2 \text{ GeV}$, FSI increases the cross section and substantially improve the description of the data; on the contrary, near the quasi-elastic peak FSI decrease the cross section, as it should be, since in agreement with the sum rule (3.18) the integral over ν must be conserved. Our results fully agree with those obtained in Ref. [16]. In the kinematics we have considered the variation of ν , from threshold to the quasi-elastic peak, corresponds to a variation of p_{lab} in the range $0.6 \text{ GeV}/c < p_{lab} < 2 \text{ GeV}/c$ (cf. the upper scale in fig. 4 and Table I) where the elastic nucleon-nucleon scattering still dominates. Note, that in this case the corresponding values of y and $|\mathbf{q}|$ change in the range $-500 \text{ MeV}/c < y \lesssim 0$ and $3.3 \text{ GeV}^2/c^2 < |\mathbf{q}|^2 < 4.3 \text{ GeV}^2/c^2$ respectively. Let us now keep y fixed and vary the values of $|\mathbf{q}|$, i.e. check the effects of FSI on the scaling function $F(|\mathbf{q}|, y)$, defined by eqs. (2.14). The results are presented in fig. 5. The dotted line is the scaling function within the PWIA, and the solid curve includes the effects of FSI. On the top horizontal axes the corresponding value of p_{lab} is also shown. At low values of $|\mathbf{q}|$ the effects of FSI are very large and no scaling behaviour can be observed. With increasing y , the scaling violation near the threshold values of $|\mathbf{q}|$, increases. This is due to the fact that a larger value of y results in a lower value of p_{lab} , in correspondence of which the elastic cross section is much higher [15]. FSI decreases with $|\mathbf{q}|$, and at values corresponding to $p_{lab} \gtrsim 1 \text{ GeV}/c$ the function $F(|\mathbf{q}|, y)$ exhibits a scaling behaviour. It should be stressed, that values of $p_{lab} \sim 1 \text{ GeV}/c$ are still in the kinematics region where the Schroedinger approach can be applied. At asymptotic

values, $|\mathbf{q}| \rightarrow \infty$, the total energy of the np -pair $\sqrt{s} \rightarrow \infty$, consequently the phase shifts δ_L in eq. (3.4) vanish and the final states $|p_{rel}; J_f L_f S_f\rangle$ become just the partial decomposition of plane waves, so that the Schroedinger approach and the PWIA coincide.

B. The Glauber approach

The inclusive cross section calculated within the Glauber approach, using the RSC and Bonn potentials, is presented in fig. 6. It can be seen that: i) the two potentials give very different results at low values of ν , ii) Glauber FSI appreciably depend upon the potential model. Our analysis shows that such a potential dependence in the kinematical region at low ν , can be explained by considering that the corrections to the deuteron S and D -waves generated by the FSI are opposite in sign. In the Glauber approach FSI are entirely driven by the distorted momentum distribution n_G^D ; let us therefore discuss the properties of the latter within the kinematical conditions relevant to y -scaling (for a detailed analysis of n_G^D at asymptotic energies see ref. [9]). It turns out that n_G^D depends upon p_{lab} , which is a function of y and $|\mathbf{q}|$. More explicitly, the p_{lab} -dependence of n_G^D arises from the p_{lab} -dependence of the parameters α and b_0 , appearing in the profile function $\Gamma_{el}(\mathbf{b})$ ((3.10)); such a dependence is shown in Figure 7. It can be seen that when the energy is high enough, ($p_{lab} \gtrsim 1.5 - 2 GeV/c$), the parameters α and b_0 become almost constant and, consequently, the distorted momentum distribution n_G^D becomes independent of the kinematics of the process. In the region $p_{lab} < 2 GeV/c$, the parameters α and b_0 exhibit a strong p_{lab} dependence, and so does the momentum distribution n_G^D . The $|\mathbf{q}|$ dependence of n_G^D calculated at $|\mathbf{p}_m| = |y|$ and $\theta_m = 0$ is shown in fig. 8. It turns out that: i) the undistorted momentum distributions n^D at large values of y strongly depend upon the potential model; ii) n_G^D exhibits a strong $|\mathbf{q}|$ behaviour at low values of \mathbf{q} ; iii) at high values of $|\mathbf{q}|$ (which correspond to high values of \sqrt{s} and p_{lab}) the distorted momentum distribution n_G^D scales to a quantity which, at large negative values of y , may differ from the undistorted momentum distributions $n^D(|y|)$ (the straight lines in fig. 8), at variance with the Schroedinger result, which predicts $n_S^D \simeq n^D(|y|)$ at high values of $|\mathbf{q}|$; iv) at high values of y the potential model dependence of $n^D(|y|)$. The explanation of points i) and ii) is clear: at low values of $|\mathbf{q}|$ the Glauber FSI is driven by the elastic cross section, which strongly decreases with $|\mathbf{q}|$; with increasing $|\mathbf{q}|$, p_{lab} reaches the inelastic threshold value ($p_{lab} \simeq 0.8 GeV/c$) and the total cross section scales to its asymptotic value $\sigma_{tot} \sim 44 mb$ ($\alpha = -0.4$, $b_0 = 0.5 fm$), and so does n_G^D . The possible reasons for the differences between the asymptotic n_G^D and $n^D(y)$ (point iii)) will be briefly discussed later on. The comparison between the Schroedinger and the Glauber approaches for the scaling function $F(|\mathbf{q}|, y)$ is shown in fig. 9. It can be seen that, for large values of y , and below the pion production threshold ($p_{lab} \simeq 0.8 GeV/c$), which is the region of existing experimental data, the Schroedinger approach provides a satisfactory description of the experimental scaling function $F(|\mathbf{q}|, y)$, unlike the Glauber approach, which overestimate the data at low $|\mathbf{q}|$ and underestimate them at high $|\mathbf{q}|$. The difference between the Schroedinger and Glauber results is strongly reduced at low values of y ($x_{Bj} \simeq 1$), where, being the target nucleon almost free, the small-scattering-angle requirement necessary for the validity of the Glauber approximation, is probably better fulfilled.

A common approximation, adopted by various authors in the Glauber type calculation of the FSI, is to consider that at $Q^2 \simeq 1 GeV^2$ the asymptotic $\sigma_{tot} \sim 44 mb$ should be used.

The validity of such an approximation is illustrated in Figure 10, where the dashed line represents the results obtained using the asymptotic $n - p$ cross section, the full lines the results with the quantities α , b_0 and $\sigma_{tot}(el)$ which properly include the dependence upon the relative momentum p_{lab} , and the dotted line the PWIA.

V. SUMMARY AND CONCLUSIONS

The aim of this paper was to address the longstanding problem of the evaluation of FSI effects in inclusive processes $A(e, e')X$, which have been described, to date, by various approximate approaches. To this end, we have considered the electro-disintegration of the deuteron, and have performed exact calculations within two different approaches to treat the final state, viz: i) the Schroedinger approach, in which, given a realistic two-nucleon interaction, the Schroedinger equation is solved to generate bound and continuum two-nucleon states, with the latter describing elastic $n - p$ rescattering, and ii) the Glauber high energy approximation, paying, in this case, particular attention to a correct treatment of the kinematics. Our aim was to understand the limits of validity of the two approaches, and to pin down the main features of the FSI mechanism, having also in mind a better understanding of these effects in complex nuclei, where calculations cannot be performed exactly. From the calculations we have exhibited, the following remarks are in order:

1) the existing experimental data on the $D(e, e')X$ process at $x_{Bj} > 1$ (negative values of y) are, to a large extent, limited to a kinematical range where the invariant mass of the final hadronic state \sqrt{s} is below the inelastic channel threshold $s \lesssim 4GeV^2$ (or $p_{lab} \lesssim 0.8GeV$) (cf fig. 9 and Table I); therefore, in spite of the large value of Q^2 involved, the two nucleons in the continuum mostly undergo elastic scattering, so that the Schroedinger approach should represent the correct description of the process and, as a matter of fact, the calculations describe the experimental data rather well.

2) The Glauber results overestimate the Schroedinger results at low values of $|\mathbf{q}|$, and underestimate them at high values of $|\mathbf{q}|$. The reason for such a disagreement between the two approaches, which is particularly relevant at large values of $x_{Bj} > 1$ (large, negative values of y), has to be ascribed to the fact that at $x_{Bj} > 1$, the direction of the ejected nucleon sizably differs from the direction of the momentum transfer.

3) At values of $s \gtrsim 4GeV^2$ (or $p_{lab} \gtrsim 1GeV$), i.e. above the pion production threshold, both the Schroedinger and the Glauber approaches might become inadequate, for the propagation of nucleon excited states (inelastic rescattering) have to be explicitly taken into account. Calculations of this type, within the approach proposed in Ref. [18], are in progress and will be reported elsewhere.

ACKNOWLEDGMENTS

This work was partially supported by the Ministero dell'Università e della Ricerca Scientifica e Tecnologica (MURST) through the funds COFIN99. Discussions with M. Braun, S. Dorkin and B. Kopeliovitch are gratefully acknowledged. L.P.K. thanks INFN, Sezione di Perugia, for warm hospitality and financial support.

REFERENCES

- [1] S. Ishikawa, J. Golak, H. Witala, H. Kamada, W. Gloeckle and D. Huber, Phys. Rev. **C57** (1998) 39.
- [2] A. Kievsky, S. Rosati and M. Viviani, Phys. Rev. Lett. **82** (1999) 3759.
- [3] N. N. Nikolaev et al., Phys. Lett. **B317** (1993) 281;
R. Seki et al., Phys. Lett. **B383** (1996) 133;
A. S. Rinat and B. K. Jennings, Nucl. Phys. **A597** (1996) 636;
L. L. Frankfurt, M. Sargsian and M. I. Strikman, Phys. Rev. **C56** (1997) 1124;
C. Ciofi degli Atti and D. Treleani, Phys. Rev. **C60** (1999) 024602;
H. Morita, C. Ciofi degli Atti and D. Treleani, Phys. Rev. **C60** (1999) 034603.
- [4] O. Benhar et al., Phys. Rev. C **44** (1991) 2328, Phys. Lett. **B359** (1995) 8;
C. Ciofi degli Atti and S. Simula, Phys. Lett. **B325** (1994) 276;
A. Rinat and M. F. Taragin, Nucl. Phys. **A598** (1996) 349;
A. Kohama, K. Yazaki and R. Seki, Nucl. Phys. **A662** (2000) 175.
- [5] J.D. Bjorken, Phys. Rev. **179** (1969) 1547.
- [6] C. Ciofi degli Atti, E. Pace and G. Salme, Phys. Rev. **C36** (1987) 1208; **C43** (1991) 1155.
- [7] S. Rock et al., Phys. Rev. Lett. **49** (1982) 1139.
- [8] T. de Forest Jr., Nucl. Phys. **A392** (1983) 232;
L. Heller and A. W. Thomas, Phys. Rev. **C 41** (1990) 2756;
U. Oelfke, P.U. Sauer and F. Coester, Nucl. Phys. **A518** (1990) 593.
- [9] N.N.Nikolaev, J. Speth and B.G.Zakharov, J. Exp. Theor. Phys. **82** (1996) 1046;
A. Bianconi, S. Jeshonnek, N. N. Nikolaev and B. G. Zakharov, Phys. Lett. **B343** (1995) 13.
- [10] S. Boffi, C. Giusti and F.D. Pacati, Phys. Rep. **226** (1993) 1.
- [11] C. Ciofi degli Atti, D. Faralli, A.Yu. Umnikov, L.P. Kaptari, Phys. Rev. **C60** (1999) 034003.
- [12] R. Machleid, K. Holinde, Ch. Elster, Phys. Rep. **149**(1987) 1.
- [13] L. Lacombe et al., Phys. Rev **C21** (1980) 861; (1995) 52.
- [14] R.V. Reid Jr., Ann. Phys. **50** (1968) 411; Phys. Rev. **C60** (1999) 034003.
- [15] A. Baldini *et al* in "Total cross Sections for Reactions of High Energy particles", Ed. H. Schopper, Springer Verlag, Berlin, 1987.
- [16] H. Arenhövel, W. Liedemann and E. Tomusiak, Phys. Rev. **C 46** (1992) 455;
G. Beck and H. Arenhövel, Few Body Systems **13** (1992) 165.
- [17] R.A. Arndt et al., "Partial-Wave Analysis Facility (SAID)", <http://said.phys.vt.edu/>
- [18] M. Braun, C. Ciofi degli Atti and D. Treleani nucl-th 0004049

FIGURES

FIG. 1. The One Photon Exchange diagram for the $D(e, e')X$ process.

FIG. 2. The PWIA diagram for the quasi elastic $D(e, e')X$ process.

FIG. 3. The FSI diagram for the quasi elastic $D(e, e')X$ process.

FIG. 4. The inclusive cross section $D(e, e')X$ versus the energy transfer ν and the laboratory momentum of the struck nucleon in the final state p_{lab} (note that the inelastic threshold corresponds to $p_{lab} \simeq 0.8 \text{ GeV}/c$). Dotted line: PWIA calculation; full line: effects of the FSI, calculated within the Schroedinger approach (3.5). The experimental data, from Ref. [7], correspond to electron initial energy $\mathcal{E} = 9.761 \text{ GeV}$ and scattering angle $\theta = 10^\circ$.

FIG. 5. The scaling function $F(|\mathbf{q}|, y)$, eq. (2.14), for various values of y vs. the three-momentum transfer $|\mathbf{q}|$ and p_{lab} . Dotted line: PWIA; solid line: FSI within the Schroedinger approach. In this and the following Figures, the values of the other relevant kinematical variables, e.g. $\nu = -M_D + \sqrt{y^2 + M^2} + \sqrt{(y + |\mathbf{q}|)^2 + M^2}$, $Q^2 = |\mathbf{q}|^2 - \nu^2$, $x_{Bj} = Q^2/2M\nu$, σ_{el} and σ_{tot} , can be found in Table I. The experimental scaling function is from Ref. [6]

FIG. 6. The inclusive cross section $D(e, e')X$ calculated within the Glauber approach. The deuteron wave function corresponds to the RSC and Bonn potentials. The experimental data are the same as in fig.4

FIG. 7. The ratio α between the imaginary to the real part of the forward elastic amplitude for np -scattering, and the parameter b_0 , eq. (3.14), used in the parameterization of the profile function (3.10). The experimental data for α are taken from [17]

FIG. 8. The dependence of the distorted momentum distribution n_G^D , eq. (3.7), upon $|\mathbf{q}|$ for various values of y and fixed values of $\theta_m = 0^\circ$ and $|\mathbf{p}_m| = |y|$. The solid line corresponds to the Reid potential and the dashed line to the Bonn potential. The dotted (dot-dashed) line represents the corresponding RSC (Bonn) undistorted momentum distributions $n(|y|)$ (eq. (2.7)).

FIG. 9. The scaling function $F(|\mathbf{q}|, y)$ vs $|\mathbf{q}|$ and p_{lab} , for various values of y , corresponding to the Glauber (full) and the Schroedinger(dashed) approaches, respectively. The dotted line represents the PWIA. The experimental data are the same as in fig.5. All curves correspond to the RSC potential.

FIG. 10. The scaling function $F(|\mathbf{q}|, y)$ vs $|\mathbf{q}|$ for various values of y and p_{lab} . The full line was obtained using in the Glauber approach the correct dependence upon p_{lab} of the quantities α , b_0 , σ_{tot} and σ_{el} , whereas the dashed line has been obtained with the asymptotic values $\alpha = -0.4$, $b_0 = 0.5 fm$ and $\sigma_{tot} = 44.2 mb$. The dotted line represents the PWIA. All curves correspond to the RSC potential.

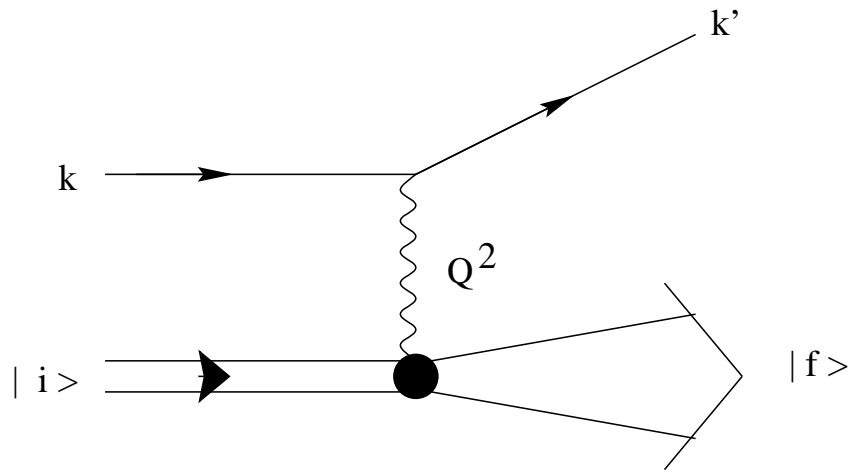


Fig. 1. C. Ciofi degli Atti....On the FSI effects....

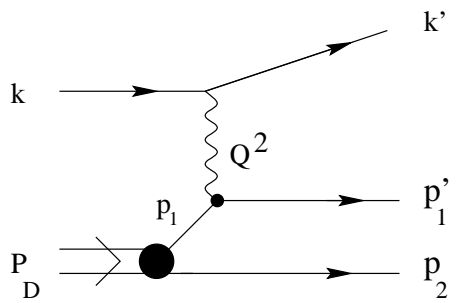


Fig. 2. C. Ciofi degli Atti....On the FSI effects....

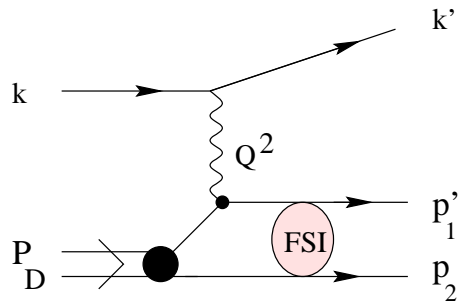


Fig. 3. C. Ciofi degli Atti...On the FSI effects...

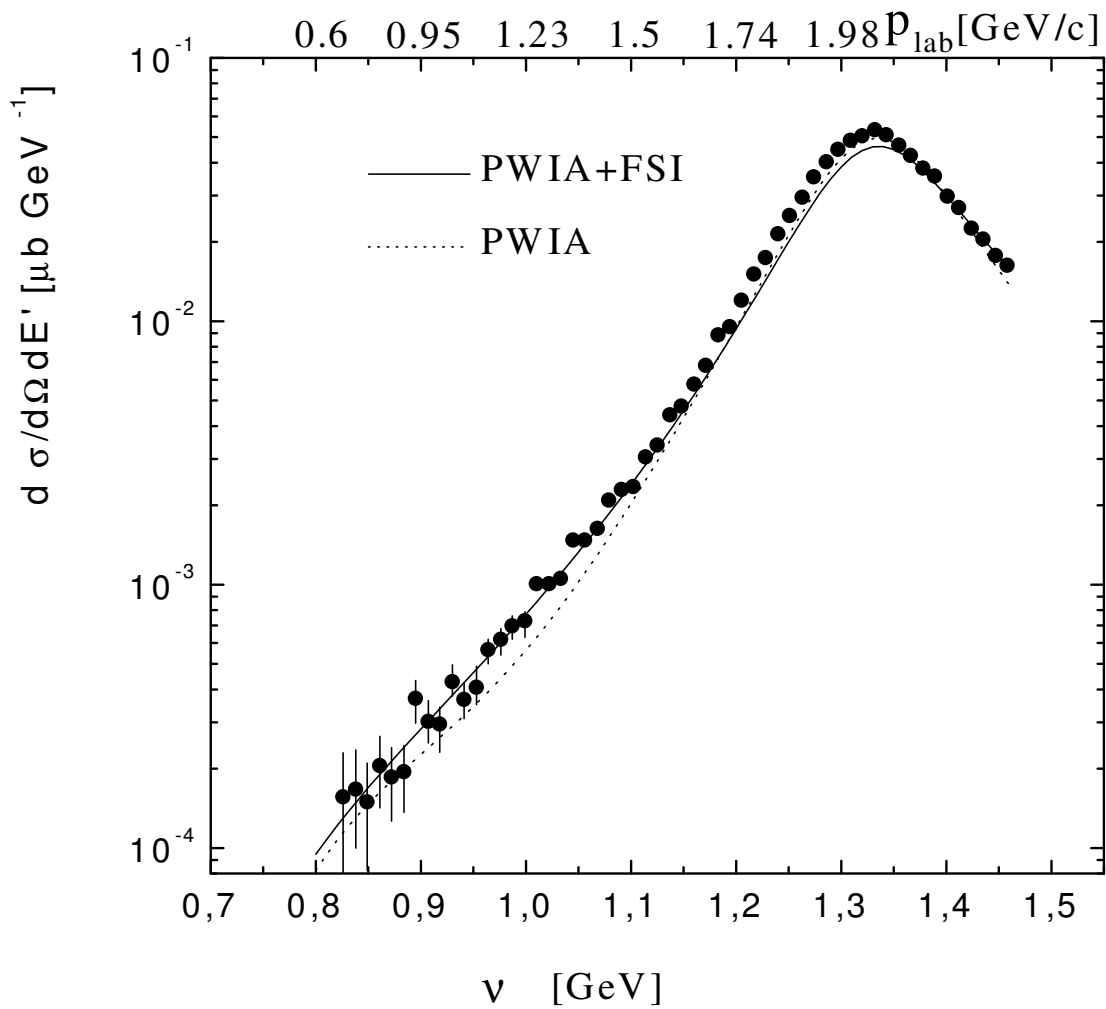


Fig. 4. C. Ciofi degli Atti....FSI effects....

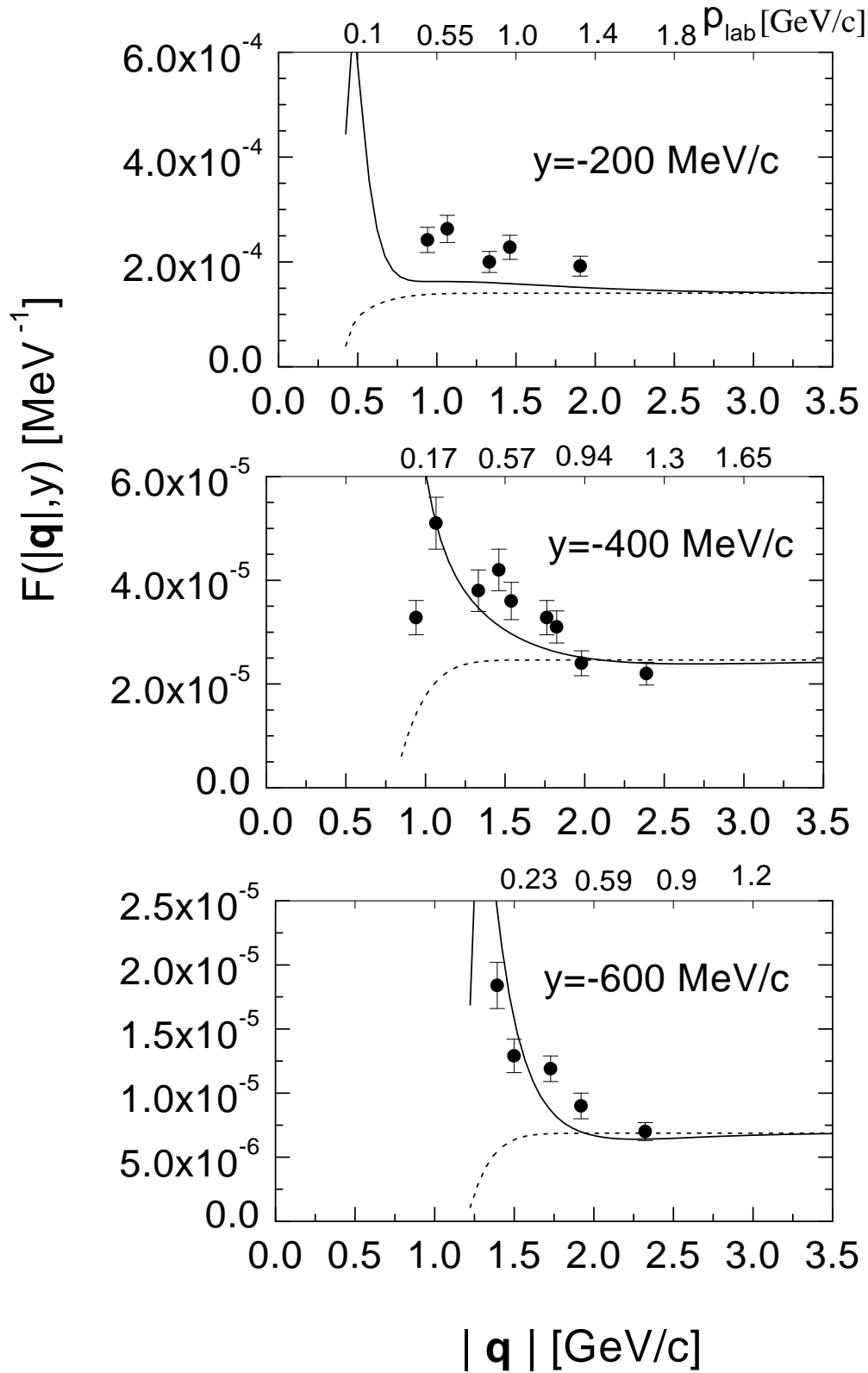


Fig. 5. C. Ciofi degli Atti....FSI effects..

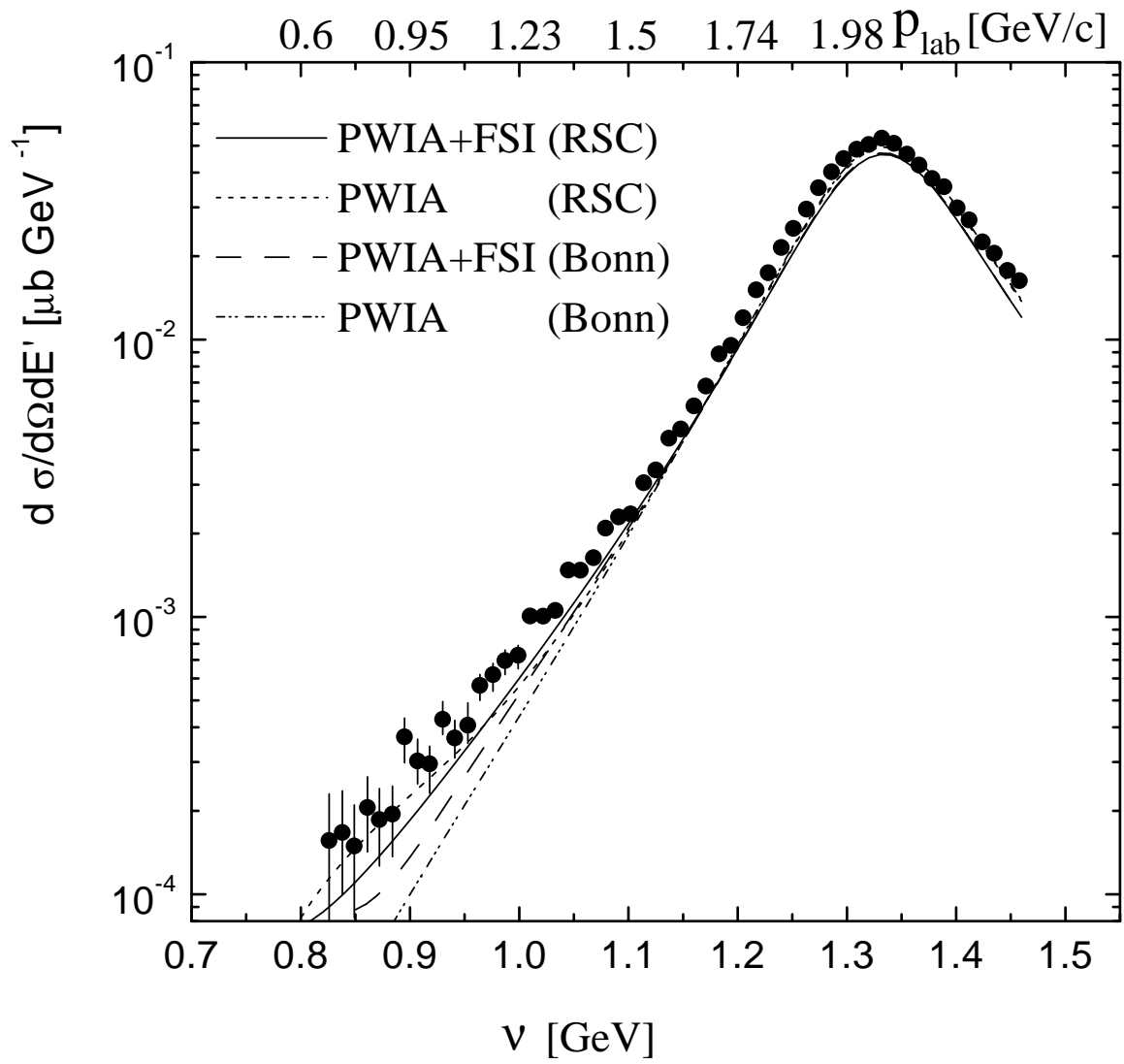


Fig. 6. C. Ciofi degli Atti....FSI effects..

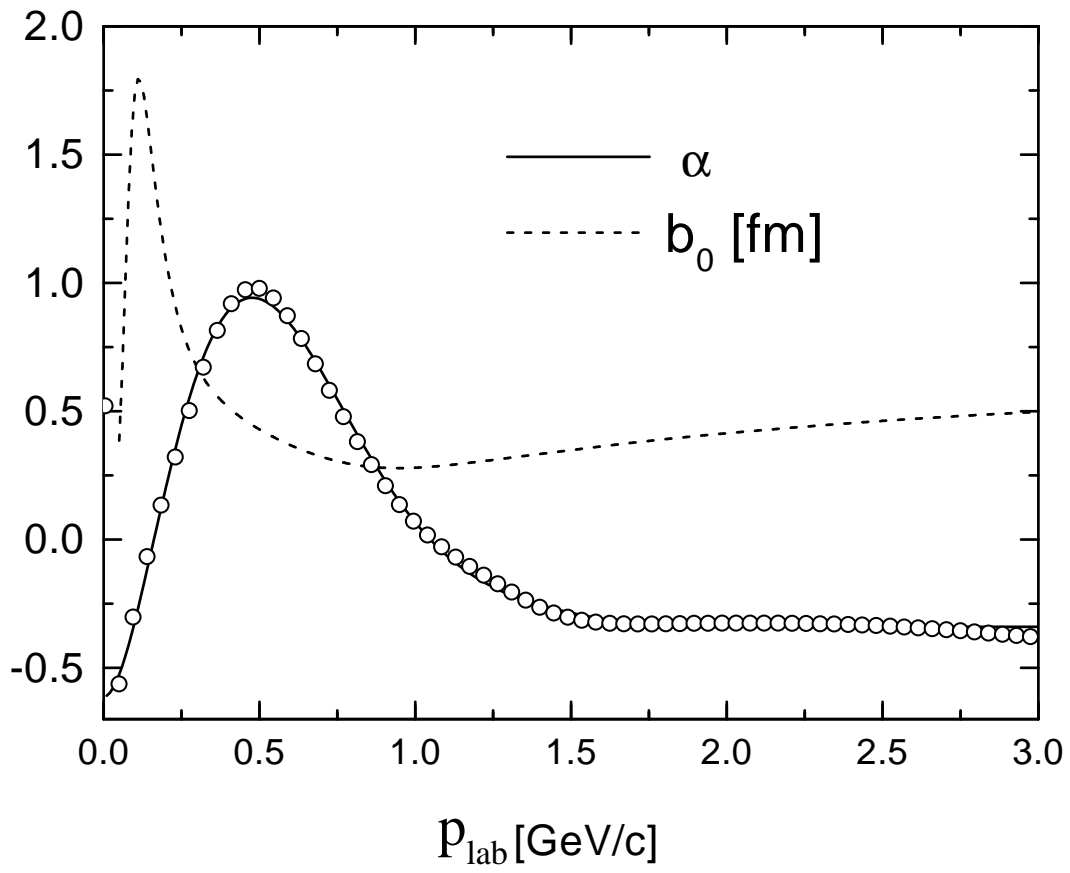


Fig. 7. C. Ciofi degli Atti....FSI effects..

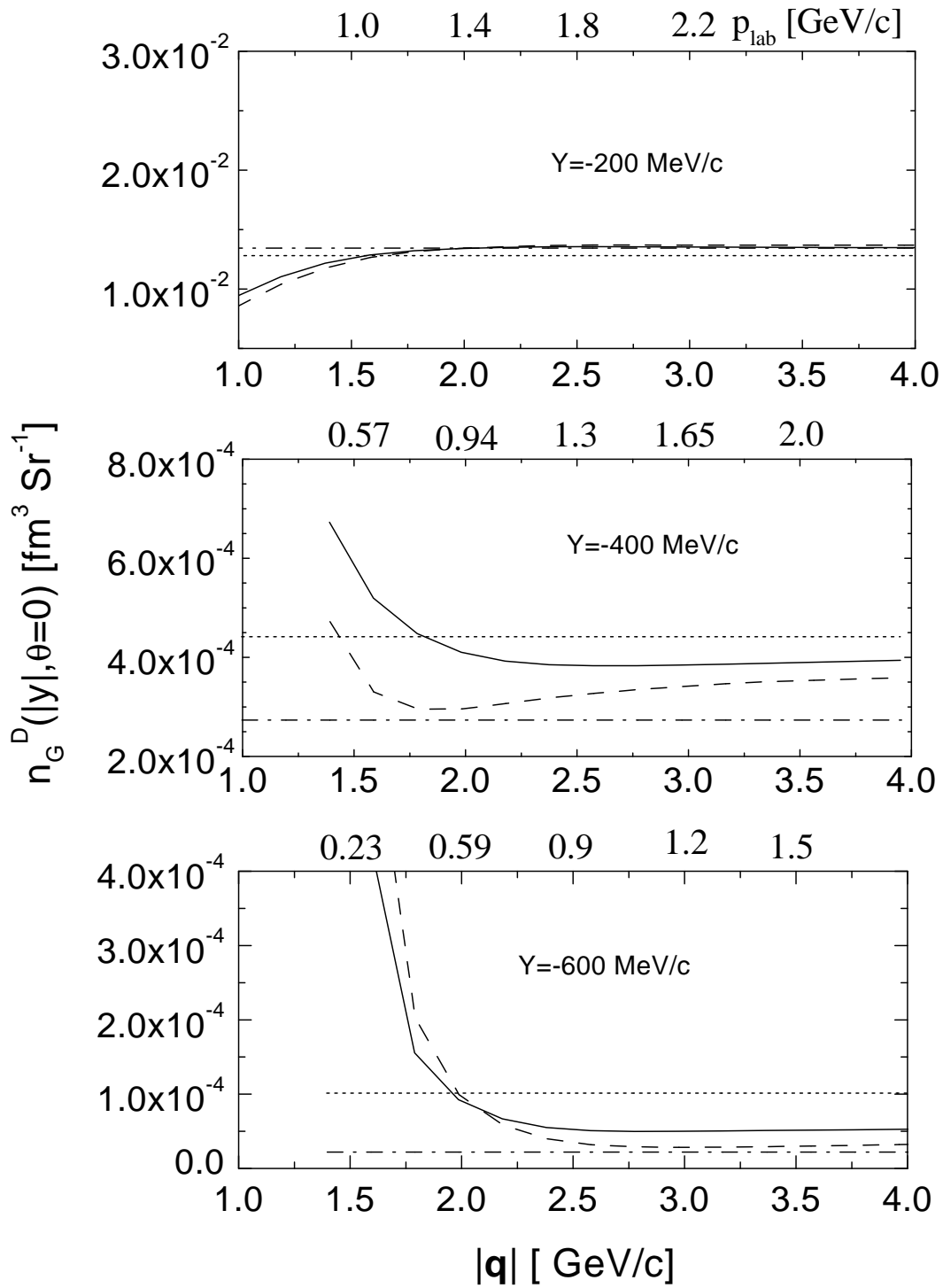


Fig. 8. C. Ciofi degli Atti....FSI effects..

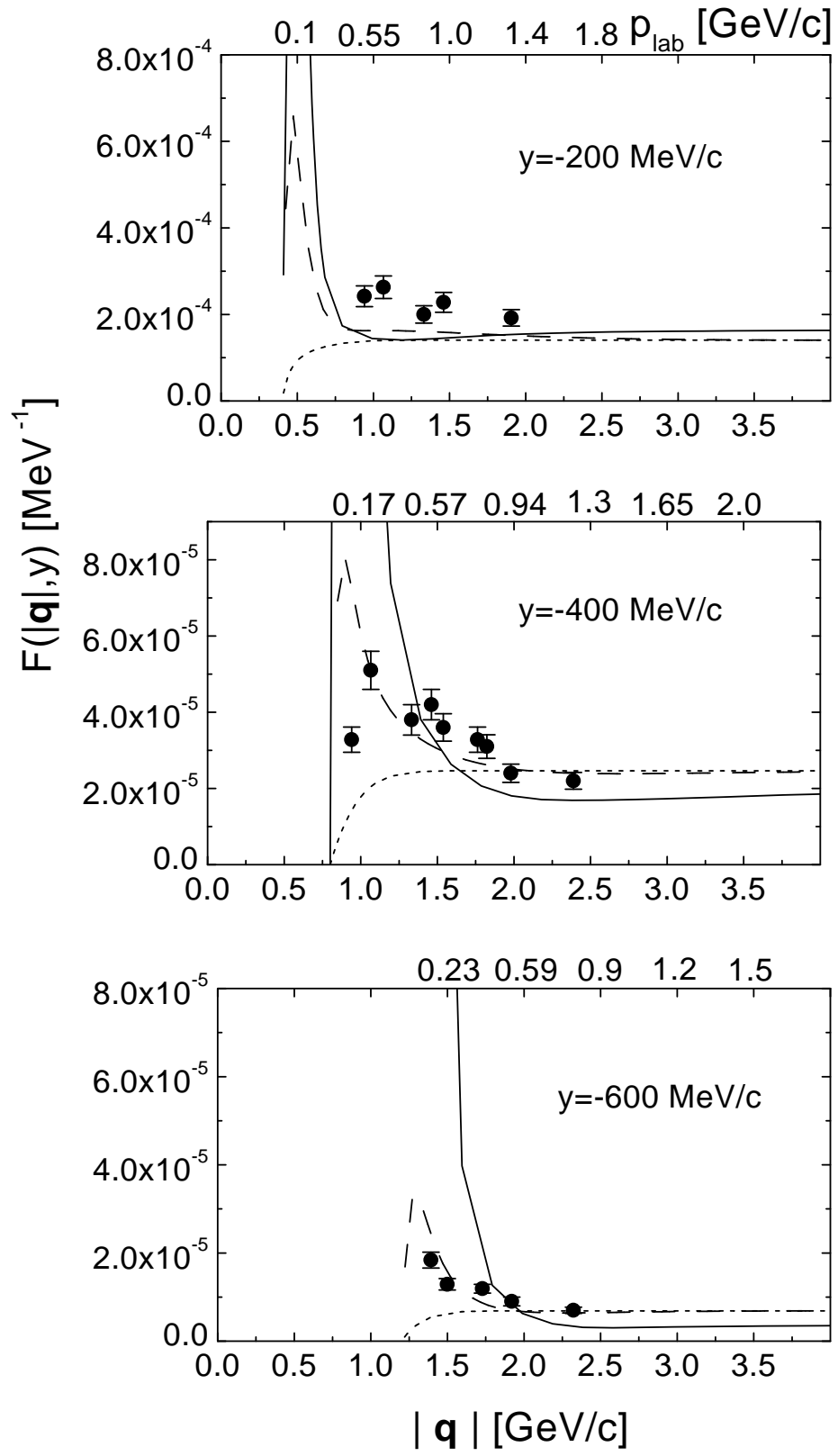


Fig. 9. C. Ciofi degli Atti....FSI effects..

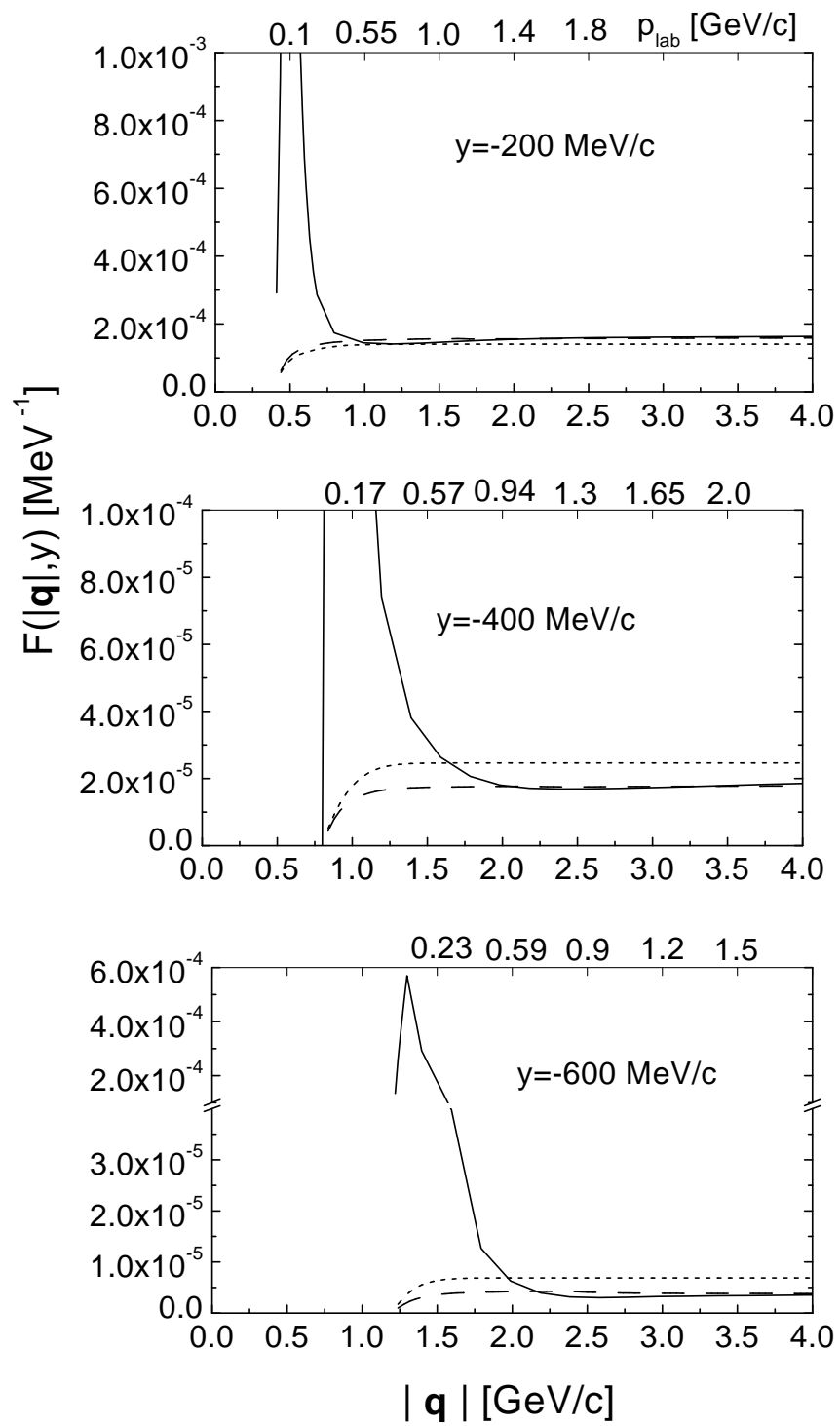


Fig. 10. C. Ciofi degli Atti....FSI effects..

TABLES

$y=-200$ MeV/c

$ \mathbf{q} $ GeV/c	ν GeV	Q^2 GeV ² /c ²	x_{Bj}	p_{lab} GeV/c	s GeV ²	σ_{el} mb	σ_{tot} mb
.50	.07	.25	1.86	.10	3.53	1744.52	1744.52
.85	.23	.67	1.58	.42	3.69	94.85	94.85
1.20	.46	1.23	1.44	.73	3.99	45.58	45.58
1.55	.73	1.87	1.37	1.03	4.37	31.96	35.71
1.90	1.03	2.56	1.33	1.32	4.81	25.85	35.78
2.25	1.34	3.27	1.30	1.62	5.27	22.44	37.06
2.60	1.66	4.00	1.28	1.90	5.74	20.29	38.57
2.95	1.99	4.74	1.27	2.19	6.24	18.82	39.99
3.30	2.32	5.49	1.26	2.48	6.73	17.76	41.19
3.65	2.66	6.25	1.25	2.77	7.24	16.95	42.17
4.00	3.00	7.00	1.24	3.05	7.75	16.32	42.92

$y=-400$ MeV/c

$ \mathbf{q} $ GeV/c	ν GeV	Q^2 GeV ² /c ²	x_{Bj}	p_{lab} GeV/c	s GeV ²	σ_{el} mb	σ_{tot} mb
.90	.21	.77	1.96	.09	3.53	2057.63	2057.63
1.25	.41	1.39	1.80	.38	3.66	109.40	109.40
1.60	.67	2.11	1.68	.66	3.91	51.82	51.82
1.95	.96	2.89	1.61	.91	4.22	35.89	36.61
2.30	1.26	3.69	1.56	1.16	4.56	28.72	35.47
2.65	1.58	4.52	1.52	1.41	4.93	24.71	36.08
3.00	1.91	5.35	1.49	1.65	5.32	22.16	37.23
3.35	2.24	6.20	1.47	1.89	5.72	20.40	38.48
3.70	2.58	7.05	1.46	2.12	6.12	19.13	39.67
4.05	2.91	7.91	1.45	2.36	6.53	18.16	40.72
4.40	3.25	8.77	1.44	2.60	6.94	17.40	41.62

$y=-600 \text{ MeV}/c$

$ \mathbf{q} $ <i>GeV/c</i>	ν <i>GeV</i>	Q^2 <i>GeV²/c²</i>	x_{Bj}	p_{lab} <i>GeV/c</i>	s <i>GeV²</i>	σ_{el} <i>mb</i>	σ_{tot} <i>mb</i>
1.30	.41	1.52	1.98	.08	3.53	2572.76	2572.76
1.65	.65	2.30	1.90	.35	3.64	129.73	129.73
2.00	.92	3.14	1.81	.58	3.83	59.87	59.87
2.35	1.23	4.02	1.75	.81	4.08	40.76	38.37
2.70	1.54	4.92	1.70	1.02	4.36	32.19	35.75
3.05	1.86	5.83	1.67	1.23	4.66	27.39	35.54
3.40	2.19	6.75	1.64	1.44	4.98	24.35	36.20
3.75	2.53	7.68	1.62	1.64	5.30	22.25	37.17
4.10	2.86	8.61	1.60	1.84	5.63	20.72	38.22
4.45	3.20	9.55	1.59	2.04	5.97	19.56	39.24
4.80	3.54	10.49	1.58	2.23	6.31	18.65	40.17

TABLE I. Kinematical variables for the inclusive $D(e, e')X$ process corresponding to the results shown in Figs 4-10. The various quantities are as follows: $|\mathbf{q}|$, ν , and Q^2 , are the energy, three-momentum and four-momentum transfers, respectively; x_{Bj} is the Bjorken scaling variable; p_{lab} is the momentum of the struck nucleon in the final state, defined by the equation $s = 2M^2 + 2M\sqrt{p_{lab}^2 + M^2}$, where s is the Mandelstam variable (cf Eq.(2.11)); finally, σ_{el} and σ_{tot} are the elastic and total cross sections used in the Glauber calculation

Table. I. C. Ciofi degli Atti....FSI effects..